The fate of smectite in KOH solutions

Andreas Bauer,[1,*] Bruno Lanson,[2] Eric Ferrage,[2] Katja Emmerich,[3] Heiner Taubald,[4] Dieter Schild,[1] and Bruce Velde[5]

[1]Forschungszentrum Karlsruhe, Institut für Nukleare Entsorgung, P.O. Box 3640, 76021 Karlsruhe, Germany
[2]Environmental Geochemistry Group, L.G.I.T., Maison des Géosciences, Université J. Fourier, B.P. 53, 38041 Grenoble Cedex 9, France
[3]Universität Karlsruhe, Institut für Mineralogie und Geochemie, Kaiserstrasse 12, 76128 Karlsruhe, Germany
[4]Universität Tübingen, Institut für Geowissenschaften, AB Mineralogie und Geodynamik, Lehrstuhl für Geochemie, Wilhelmstrasse 56, 72074 Tübingen, Germany
[5]Ecole Normale Supérieure, Département de Géologie, 24, rue Lhomond, 75231 Paris Cedex 05, France

Abstract

The aim of the present study was to investigate the detailed evolution of the SAz-1 smectite in 1 *M* KOH at 80 °C at a solid/liquid ratio of 1/80. AFM observations indicated no change in crystal size or shape. XRD measurements at 40% relative humidity revealed changes in expandability of the smectite. The (001) reflection profile of smectite was modeled using a trial-and-error approach. The results indicate that with increasing run time, the number of non-expandable layers with zero or one water layer increases and that the coherent scattering domain size of the smectite decreases. IR spectroscopy of the reacted smectite suggests that there is no change from the initial clay products. The dehydroxylation temperature showed a slight decrease from 619 to 605 °C. STA measurements demonstrated that the cis-vacant character of the octahedral sheet remained nearly unchanged throughout the experiment. Determination of the average layer charge showed a continuous increase from 0.32 to 0.42 eq/$(Si/Al)_4O_{10}$, whereas the layer charge distribution indicated the appearance of high charged smectite layers with a charge of ~ 0.6 eq/$(Si/Al)_4O_{10}$ and the disappearance of the low charged layers. XPS and SEM measurements indicate an increase of Al in the smectite samples. Isotope data support the theory of an internal diffusion mechanism by gradual changes in $\delta^{18}O$ values.

From these data it appears that KOH solutions provoke a mineralogical change in the 2:1 layer of the smectite minerals that increases the layer charge by increasing the Al content. This mineralogical change does not involve dissolution/crystallization processes and then must show solid-state transformation of the clays at 80 °C.

Keywords: Smectite, illitization, solid-state transformation, KOH

Introduction

In 1997, at the end of a workshop dedicated to Victor Drits by the French Clay Group, Bernard Kübler proposed that it would be a great help if the speakers would give their definitions of vermiculite, high-charge smectite, and illite at the beginning of their talks. As a matter of fact, a look through the literature reveals that the terms used for expandable layers in the smectite-to-illite reaction are just operationally defined and, as such, they do not necessarily coincide with definitions from the nomenclature committee of the Association international pour l'etude des argiles. The aim of our study was to investigate the fate of smectite during a possible smectite-to-illite transformation. The question, then, is whether smectite is just a passive partner in the reaction giving the ingredients for the new phase illite? Or is illite perhaps smectite with a higher charge, and smectite collapse occurs only when K^+ is supplied to the high-charge interlayer sites?

Chemical compositions of diagenetically altered shales, sandstones, or bentonites studied by Srodon et al. (1986), Nadeau and Bain (1986), Awwiller (1993), and Cuadros and Altaner (1998) indicate the formation of high-charge expandable layers together with the illitization process. The experimental illitization of smectite indicates that the proportion of high-charge layers increases followed by K fixation and subsequent illitization (Whitney and Northrop 1988). The high-charge but exchangeable layers are similar to the vermiculitic component described by Shutov et al. (1969) and Drits et al. (1997). As a result, a randomly interstratified illite/smectite (R0 I/S) mixed-layer structure has three components: one fully expandable (smectite), one partially expandable (vermiculite), and one non-expandable (illite). This means that the smectite-to-illite transformation first must involve the vermiculitization of the smectite layers through the formation of high-charge, tetrahedrally substituted layers from the original clay (Drits 1985). Meunier et al. (2000) described this process as the vermiculitization of smectite interfaces. In their model, the low-charge montmorillonite is transformed into a high-charge vermiculite that remains partly expandable (one water layer or one ethylene glycol layer at 80% relative humidity) if the interlayer is not K^+- or NH_4^+-saturated. A vermiculite interlayer leads to the formation of illite when K or NH_4^+ is supplied. But how are smectite particles transformed during their transition to R0 I/S? Two processes may control the reaction: solid-state transforma-

* E-mail: bauer@ine.fzk.de

tion (Shutov et al. 1969; Dunoyer de Segonzac 1970; Hower et al. 1976), or dissolution/crystallization (Altaner and Ylagan 1997; Baronnet 1997). Many studies have reported evidence supporting one or the other reaction mechanism.

In the literature, two experimental pathways are commonly used to obtain illite from a smectite precursor. One is to use KCl and high temperatures (>200 °C) and pressures, and the other is to use KOH at low temperatures (<100 °C). Hydrothermal synthesis experiments have formed R0 I/S from smectite at elevated temperatures (e.g., Robertson and Lahann 1981; Whitney and Northrop 1988). Reactions in KOH solutions lead to a decrease of the coherent scattering domain size of the smectite followed by the illitization of the smectite and, finally, the formation of pure illite (e.g., Eberl et al. 1986, 1993; Bauer and Velde 1999). In the present study, we focus on the KOH system. The aim of the present manuscript is to follow the fate of a fully expandable and low-charge smectite before it becomes illite in KOH solutions with different experimental techniques.

MATERIALS AND METHODS

Starting clay

The starting clay mineral for this experimental study was a purified homoionic montmorillonite obtained from the SAz-1 source clay material (Clay Minerals Society, Purdue University, http://www clays org/sourceclays/SourceClays html) First, the clay was conditioned to remove soluble salts, sparingly soluble minerals, and trace cation impurities after the procedure proposed by Bauer and Velde (1999) The purified smectite was converted into its Na form (Moore and Reynolds 1997), and the <1 μm fraction of smectite was separated by sedimentation techniques (Day 1965) X-ray diffraction (XRD) analysis for the conditioned clay revealed that montmorillonite is present at 100% Finally, the clay separate was converted into its K form

Starting solution

The solutions were prepared from analytical grade chemicals A Milli-Q Reagent Water System from Millipore Corp provided deionized water (DI) with a resistivity of >18 MΩ/cm

Experimental protocol

Smectite samples weighing 2 g were added to 160 mL of a 1 *M* KOH aqueous solution Reactions were conducted in HDPE Nalgene bottles kept in ovens at 80 °C with reaction times lasting up to 150 days The bottles were shaken twice a week At the end of an experimental run, the bottles were removed, quenched in cold water (25 °C), and opened The supernatant was filtered through a 0 1 μm Nucleopore membrane into cleaned polypropylene bottles and analyzed The solid material was then washed carefully five times with 150 mL of DI water After washing the material, it was resuspended five times for 1 min in an ultrasonic bath in 150 mL of a 1 *M* $SrCl_2$ solution Saturation with Sr^2 was used to ensure the presence of two water layers in the expandable layers under XRD data collection conditions (see below) To promote complete cation exchange, the suspensions were stored after the ultrasonic treatment for 4 h at 50 °C After this procedure, the sample was washed five times with 150 mL of DI water After washing the samples, one part of the solid was used to prepare the XRD slide and the rest was converted into the Na form and freeze dried for layer charge, oxygen isotope, and XPS measurements, as well as for thermal analysis

X-ray diffraction

The evolution of clay mineral structure and the formation of secondary phases were monitored by XRD Oriented slides were prepared by pipetting a slurry of Sr-saturated samples on a glass slide and drying it at room temperature for a few hours to obtain an air-dried preparation XRD scans were recorded on a Bruker D5000 diffractometer (Cu radiation at 40 kV and 40 mA) equipped with an Ansyco rh-plus 2250 humidity control device coupled to an Anton Paar TTK450 chamber The measurement range was from 2 to 50° 2θ, with a step size of 0 04° and 6 s counting time The divergence slit, the two Soller slits, the antiscatter slit, and the resolution slit were 0 5, 2 3, 2 3, 0 5, and 0 06°, respectively All XRD analyses were conducted at a relative humidity of 40% after a homogenization period of about 15 min before the measurement

The (001) reflection profile of SAz-1 smectite was modeled using the algorithms developed initially by Sakharov and Drits (1973), Drits and Sakharov (1976), Drits et al (1997), and Sakharov et al (1999a) In addition, smectite hydration heterogeneity was monitored using the methodology developed by Ferrage et al (2005) This heterogeneity results from the coexistence in the same crystal of the different layer types usually considered in the smectite structure in non-saturated water vapor conditions: dehydrated layers (0W layers, layer thickness at 9 6–10 1 Å), mono-hydrated layers with one plane of H_2O molecules in the interlayer (1W layers at12 3–12 7 Å), and bi-hydrated layers with two planes of H_2O molecules in the interlayer (2W layers at 15 1–-15 8 Å) Such structural heterogeneity can be seen as the result of both contrasted layer charges from one layer to the other or within a single layer and intrinsic thermodynamic effects

For the modeling of all experimental XRD patterns, the preferred orientation of the sample (σ*) was set to 7° Because the water content of hydrated layers cannot be determined accurately from the sole (001) reflection, the number of H_2O molecules was set to 3 and 6 $H_2O/O_{20}(OH)_4$ in 1W and 2W layers, respectively Other structural parameters and atomic positions in the different layer types were described in Ferrage et al (2005)

Briefly, the fitting strategy developed by Ferrage et al (2005), based on algorithms of Sakharov et al (1999b), consists of using a main structure, periodic when possible, to reproduce as much as possible of the experimental XRD pattern If necessary, additional contributions to the diffracted intensity are introduced to account for the misfit between calculated and experimental patterns The presence of two mixed-layer structures (MLSs) does not imply that two populations of particles are physically present in the sample Therefore, layers with the same hydration state present in the different MLSs contributing to the diffracted intensity are assumed to have identical properties (chemical composition, layer thickness, z-coordinates of atoms) The relative proportions of the different MLSs and that of the different layer types in these MLSs were also considered as variable parameters during the fitting procedure

Powder XRD patterns were recorded using a Bruker D5000 powder diffractometer equipped with a BSI (Baltic Scientific Instrument) Si(Li) solid detector, and Cu*K*α radiation Intensities were recorded from 56 to 65° 2θ, using 0 01° 2θ steps, and a 50 s counting time per step

Layer charge

A detailed description of the experimental protocol and the layer-charge determination can be found in Mermut and Lagaly (2001) and Hofmann et al (2004) All measurements were done in triplicate

X-ray photoelectron spectroscopy

X-ray photoelectron spectroscopy (XPS) analyses were performed using a Physical Electronics Inc PHI 5600ci spectrometer equipped with a hemispherical capacitor analyzer and multichannel detector Si 2s, Al 2p, and Mg 2s elemental lines were recorded by Al*K*α X-ray excitation (1486 6 eV) using a source power of 200 W, a source-sample distance of 10 mm and a source-analyzer angle of 54° The angle between the sample surface normal and the analyzer was 45° Atomic concentrations were calculated from peak areas of elemental lines after Shirley background subtraction, by use of sensitivity factors and the analyzer transmission function determined at same acquisition conditions Calibration of the Si, Al, and Mg analyses was done using synthetic SiO_2, Al_2O_3, and $MgAl_2O_4$ samples The SiO_2 (30 nm SiO_2 layer on a silicon wafer), Al_2O_3 (sapphire single crystal, TBC-Kelpin Co , Neuhausen), and $MgAl_2O_4$ (99 985% $MgAl_2O_4$ powder, Alfa Aesar) samples were purified with ethanol and afterward sputtered with Ar ions for 10 to 80 s Based on the measurements of the ultra-pure solids, the PHI Multipak sensitivity factors were refined for the Al*K*α X-ray excitation The detection limit of the Si, Al, and Mg analyses is 0 5 mol%

Simultaneous thermal analysis

The measurements were performed on a simultaneous thermal analysis (STA) 449 C Jupiter from NETZSCH-Gerätebau GmbH with a TG/DSC sample holder The STA is connected with a quadruple mass spectrometer 403 C Aëolos from IPI/InProcess Instruments/NETZSCH-Gerätebau GmbH All samples were allowed to equilibrate at a relative humidity of 53% in a dessicator above a saturated $Mg(NO_3)_2$ solution for at least 48 h The conditions for the STA measurement are reported in Table 1

Infrared spectroscopy

The IR spectra were recorded with a Perkin-Elmer 1760 spectrometer over the range 4000–400 cm^{-1} (optical resolution, 2 cm^{-1}) The pellets were prepared after dilution of 1 mg of sample in 100 mg of KBr

Atomic force microscopy measurements

Both a raw sample of SAz-1, and samples of SAz-1 recovered from experiments were observed by atomic force microscopy (AFM) A dilute suspension of each SAz-1 Na-saturated sample was gently sonicated and centrifuged onto a crystal of highly ordered pyrolytic graphite (HOPG) The excess aqueous solution was removed and the sample dried in an oven at 40 °C A Veeco Instruments DIMENSION 3100 AFM with Nanoscope IV controller operating in tapping mode was used for imaging the smectite particles under ambient conditions in air (after drying) High aspect ratio Si single-crystal AFM tips were used The nominal oscillation resonance frequency of the cantilever was 283 kHz The maximum scan rate was 5 Hz The smectite particle morphology and dimensions were evaluated quantitatively using the Image WSXM 2 0 software (NANOTEC) Using AFM, we analyzed smectite particles lying flat on the HOPG substrate Aggregates of randomly oriented smectites were disregarded in the measurements

Scanning electron microscopy

Scanning electron microscopy (SEM) was used to observe material of which there was too little to analyze by XRD The SEM photographs were obtained using a JEOL GSM-6100 instrument with a KEVEX energy dispersive spectrometer used for semi-quantitative analysis (peak height ratios)

Oxygen-isotope analyses of clays

The oxygen-isotope composition of the smectite samples was measured at the University of Tübingen, using a conventional extraction of oxygen and BrF_5 reagent, according to a method adapted from Clayton and Mayeda (1963) About 7 mg of sample were used and the extracted oxygen was converted to CO_2 The sample was wrapped in aluminum foil and dried for 3 days in a desiccator with P_2O_5 to remove non-structural water (Savin and Epstein 1970) Then the samples were loaded immediately (within seconds) into the Ni-reaction vessel in a dry N_2 stream and pumped for at least 2 h at temperatures below 180 °C before BrF_5 was added Reaction was performed at 550 °C for 16–18 h Isotope measurements were made using a Finnigan MAT isotope ratio mass spectrometer (Finnigan MAT 252) Oxygen-isotope compositions are given in the standard δ-notation, expressed relative to VSMOW in per mil (‰) The precision of $\delta^{18}O$ values was better than 0 2‰ when compared to the reference $\delta^{18}O$ values for NBS-28 of 9 64‰

The 1 *M* KOH fluid was analyzed for total oxygen-isotope composition (H_2O + KOH) using a TC-EA preparation device connected online to a Finnigan MAT Delta + XL continuous-flow mass spectrometer 0 5 µL liquid was placed in a silver container and combusted at 1450 °C The analytical precision is better than ±0 3‰

Solution compositions

Concentrations of dissolved Si, Al, K, Fe, and Mg were determined for all samples The Si and Al were analyzed using a Plasma 400 ICP-AES (Perkin Elmer) All measurements were done in triplicate

Results

XRD

For Sr-saturated specimen SAz-1, the position of the 001 reflection is ~15.3 Å (Fig. 1). With increasing reaction time, the profile of this reflection is slightly broadened and becomes asymmetrical on the high-angle side. Profile broadening may be related to a decrease of the coherent scattering domain size but the asymmetry on the high-angle side of the (001) reflection is more likely attributed to the presence of layers with lower layer thickness. The increased proportion of these layers is best revealed by XRD profile modeling. Structure models and structural parameters used to fit the (001) reflection are reported in Table 2. In agreement with structure models determined by Ferrage (2004) on the <1 µm fraction of Sr-saturated SAz-1, two MLSs were used to reproduce the (001) reflection. The first one

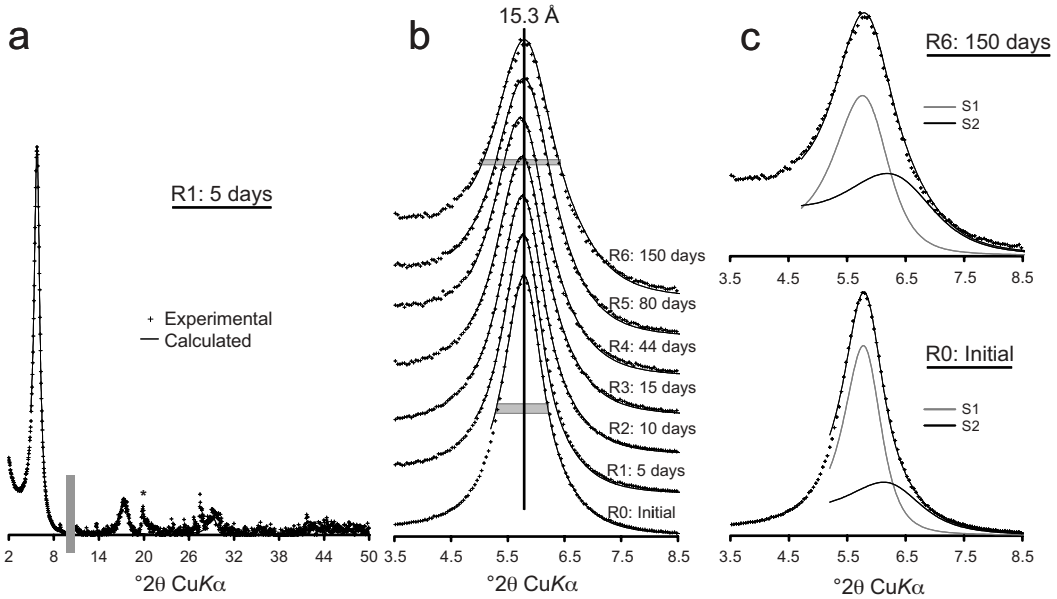

Figure 1. X-ray diffraction profile modeling of reacted Sr^{2+}-saturated SAz-1 recorded at 40% relative humidity. (**a**) Comparison between experimental (crosses) and calculated (solid line) XRD patterns for R1 sample over the whole angular range (2–50° 2θ). The gray bar indicates a modified scale factor for the high-angle region (×10) whereas * indicates *hk*0 bands. (**b**) Evolution of the (001) reflection for the complete series and comparison with the corresponding calculated profile. The gray bars outline the modifications in peak width between 5 days and 150 days of reaction time. (**c**) Example of decomposition showing the contribution of the two structures (see Table 1 for details). XRD patterns (experimental and calculated) for initial R0 sample are from the study of Ferrage (2004).

is mainly composed of 2W layers with minor 1W layers (S1), whereas the second one is more heterogeneous and incorporates the three layer types (S2).

XRD measurements at 40% RH of the Sr-saturated samples reveal some changes in the smectite expandability. With increasing alteration time, the compositions of the two MLSs remain constant except for the last two samples in which an increase of 1W layers was observed in both contributions. A modification in expandability was observed, mainly induced by the increase of the S2:S1 ratio for reaction times up to 45 days (Table 2). As a result, the number of 1W layers increases whereas that of 0W layers seems to be about constant with reaction time. The layer thickness of the different layer types were found constant whereas CSDS of the crystals decreased from 5.4 to 4.3 after 45 days and then remained constant till the end of the experiment (Table 2). Some $SrCl_2$ and $SrCO_3$ peaks were found as impurities resulting from the Sr^{2+}-saturation procedure. In addition, low-intensity sharp peaks, likely attributed to zeolite-type minerals (phillipsite), were observed in reacted samples.

Observation of the (060) peak region gives information on the phyllosilicate structures in the **a**-**b** plane. This region was monitored as a function of reaction time (Fig. 2). The appearance of a small peak at 1.54 Å beside the initial peak at 1.49 Å indicates the formation of trioctahedral domains (Brindley and Brown 1980). A similar observation was made by Beaufort et al. (2001) under neutral pH conditions at higher temperatures (100 and 200 °C). In addition, there is a clear shift in the position of the (060) peak of the major phase toward higher *d*-spacings. This shift indicates a change in the internal structure of the aluminous smectite. Such a shift is indicative of an increase in layer charge, either for beidellite or montmorillonite substitutions in the lattice (Velde 1985).

TABLE 1. Conditions of the STA measurement

	DSC/TG/MS
Sample amount	50 mg
Grain size	powder
Packing density	loosely packed, no pressing
Reference material	Empty crucible with lid
Furnace atmosphere	50 mL/min air + 20/mL/min N_2
Crucibles	Pt with lid
Thermocouples	$Pt/Pt_{90}Rh_{10}$
Heating rate	10 K/min
Temperature range	35–1000 °C

Solution chemistry

The changes in solution composition with time were monitored during the reaction. Due to the high KOH content, no significant variation of pH has been observed. After a strong initial increase of the Al and Si concentration in solution, the concentration increase flattens out to remain constant within the error of the measurement at ~950 mg/L for Si and ~250 mg/L for Al (Fig. 3). With increasing reaction time, the Al/Si ratio in solution decreases from 0.39 to 0.25. The solution concentrations of Mg and Fe were about 0.06 and 0.3 mg/L, respectively, throughout the experiment.

The pH and aqueous species, as well as the saturation index of possible precipitates, were calculated at in-situ conditions by using the EQ3/6 software package (Wolery et al. 1988) and the SUPCRT92 database (Johnson et al. 1992). The in situ pH was determined by calculating the charge balance on H^+. We checked that the presence of small amounts of other cations does not change the pH calculations, given the high K concentrations.

Layer charge

We observed a continuous evolution of the layer charge with increasing reaction time. We measured a mean layer charge of 0.32 eq/$(Si,Al)_4O_{10}$ for the initial SAz-1, which is in agreement with the value reported by Mermut and Lagaly (2001) but lower than the value reported by Jaynes and Bigham (1987). The mean layer charge increases from 0.36 eq/$(Si,Al)_4O_{10}$ after 5 days to 0.42 eq/$(Si,Al)_4O_{10}$ at the end of the experiment (Fig. 4a). The initial SAz-1 shows a heterogeneous charge distribution containing ~4% of layers with a charge >0.4 eq/$(Si,Al)_4O_{10}$ (Fig. 4b). With increasing run time the layer charge distribution is shifted toward higher charge densities. After 150 days more than ~37% of the smectite layers have a charge higher than 0.4 eq/$(Si,Al)_4O_{10}$ (Fig. 4b).

XPS/SEM

The Al/Si and the Mg/Si atomic ratios of the Na-saturated solids were measured to follow changes in smectite chemistry as a function of reaction progress. Both ratios increase as a function of reaction time indicating the increase of Al and Mg in the smectite structure. The Al/Si atomic ratio as a function of a reaction time increased from 0.39 to 0.48 after 150 days (Fig. 5).

TABLE 2. Optimum structural parameters used for the simulation of XRD profiles

Sample	S cont.	2W	1W	0W	LT 2W	LT 1W	LT 0W	N	Tot. 2W	Tot. 1W	Tot. 0W
Initial	S1:62	92	8	0	15.30	12.32	10.00	5.5	75	18	7
	S2:38	47	35	18							
Reactor 1: 5 days	S1:66	92	8	0	15.30	12.32	10.00	5.4	77	17	6
	S2:34	47	35	18							
Reactor 2: 10 days	S1:64	92	8	0	15.30	12.32	10.00	4.9	76	18	6
	S2:36	47	35	18							
Reactor 3: 15 days	S1:58	92	8	0	15.30	12.32	10.00	4.6	73	19	8
	S2:42	47	35	18							
Reactor 4: 44 days	S1:58	92	8	0	15.30	12.32	10.00	4.3	73	19	8
	S2:42	47	35	18							
Reactor 5: 80 days	S1:57	85	15	0	15.30	12.32	10.00	4.3	69	23	8
	S2:43	47	35	18							
Reactor 6: 150 days	S1:51	85	15	0	15.30	12.32	10.00	4.3	63	27	10
	S2:49	40	40	20							

Notes: The relative contribution (S cont.) of the two structures S1 and S2 is given in % as well as the proportion of bi-hydrated, mono-hydrated, and dehydrated layers (2W, 1W, and 0W layers, respectively) within these elementary contributions. The total proportion of 2W, 1W, and 0W layers in crystal is given in % as Tot. 2W, Tot. 1W, and Tot. 0W, respectively. Layer thickness (LT) of the different layer type is given in angstroms. N is the mean number of layers in the coherent scattering domain. The structure model of initial sample is given from the study of Ferrage (2004).

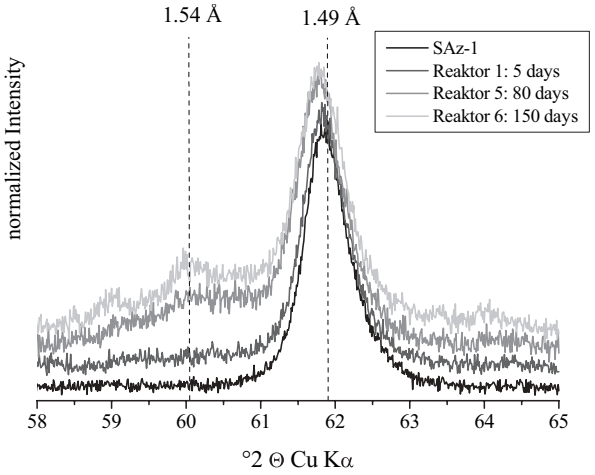

FIGURE 2. Evolution of the (060) bands as a function of reaction time.

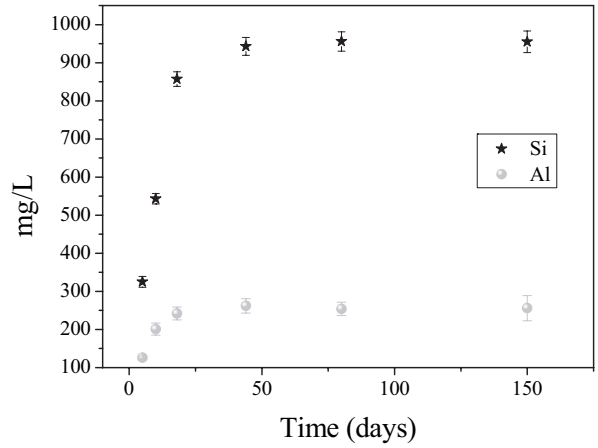

FIGURE 3. Plot of the released Si and Al concentrations as a function of the pH for 25, 60, and 80 °C. Error bars correspond to the standard deviation of triplicates.

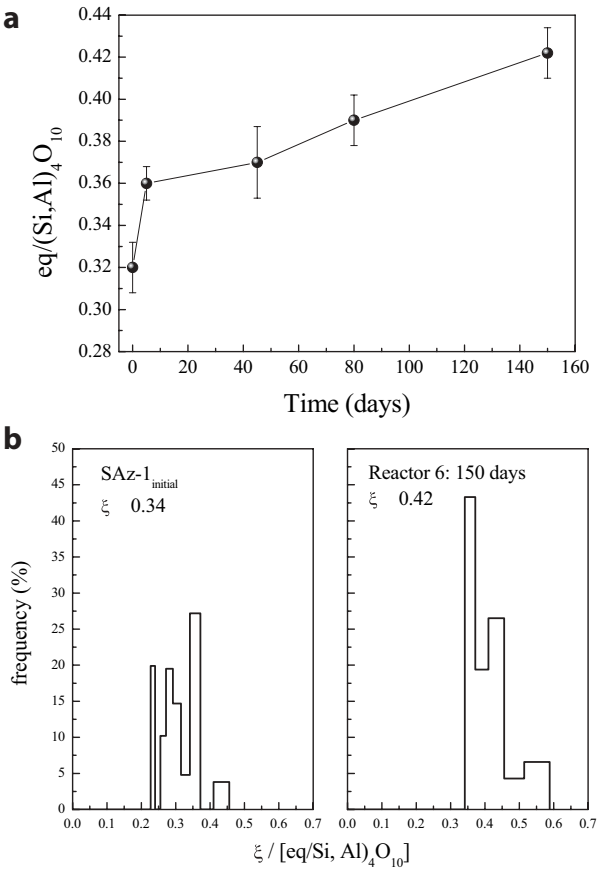

FIGURE 4. (**a**) Evolution of the layer charge as a function of reaction time. Error bars correspond to the standard deviation of triplicates. (**b**) Plot of the evolution of the layer charge distribution of the initial SAz-1 smectite and after 150 days reaction time.

The Mg/Si ratio increased from 0.17 to 0.3 after 150 days (Fig. 5). The initial values of 0.39 and 0.17 measured on the initial smectite are in perfect agreement with the values measured by Metz et al. (2005a) for SAz-1 montmorillonite. SEM observations were carried out to verify the formation of precipitated Al- or Mg-bearing phases that are below the detection limit of XRD. Some rare small brucite crystals but no Al-bearing phases were found after 80 days of reaction time. Although the information depth of the XPS signal is 6.3 nm, it cannot be concluded, a priori, that XPS analyses only a surface layer of around five smectite layers. Homogenously distributed contaminants may be detected by the XPS signal as well because the analyzed sample area is about 1 mm^2. However, accessory minerals that are within a smectite aggregate or covered by a smectite coating would not be included in the XPS analysis. Some $SrCl_2$ impurities were found by SEM and during XPS analysis.

STA measurements

For the STA measurements, we used Na-saturated samples. Based on the dehydroxylation temperature of 643 °C, the SAz-1 is a *cis*-vacant (cv) smectite (Drits et al. 1995; Emmerich et al. 2001). With increasing reaction time, the dehydroxylation temperature decreases continuously to 605 °C after 150 days (Fig. 6). In addition, a second (small) dehydroxylation peak occurred at about 790 °C after 80 days of reaction time that may be attributed to a trioctahedral smectite.

The dehydration temperature of the initial Na-saturated smectite was measured to be 147 °C. For the first 80 days, the dehydration temperature varies within the error of the measurement. After 150 days, the dehydration reaction splits and a second maximum at 127 °C was observed in DSC curves (Fig. 6). TG measurements demonstrate that the amount of interlayer water increased from about 12% for the untreated Na-saturated SAz-1 to about 17% after 150 days of reaction.

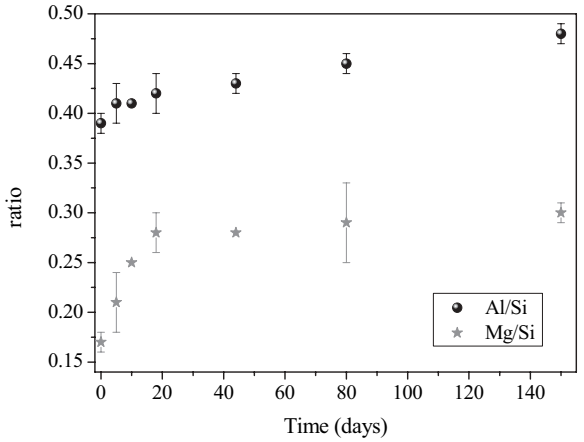

FIGURE 5. Plot of the Al/Si ratio of the clay from XPS as a function of reaction time. Error bars correspond to the standard deviation of triplicates.

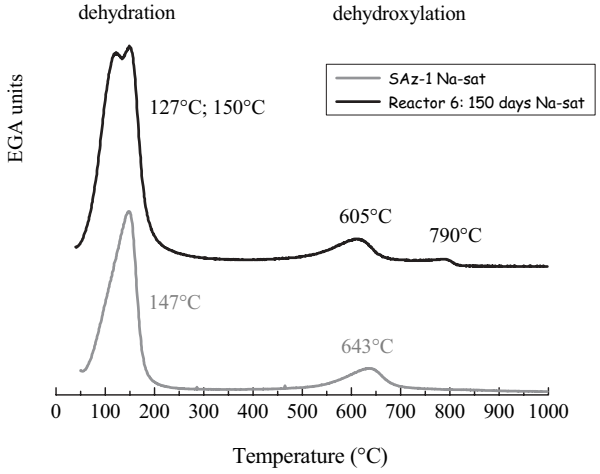

FIGURE 6. MS curves of the evolved water (m/e = 18) during STA measurement

Infrared

IR spectroscopy revealed unchanged smectite spectra for all the experiments. No loss of intensity of vibration bands as a function of reaction time was observed. A weak band at 792 cm^{-1} indicating traces of poorly crystalline silica (Madejova and Komadel 2001) disappeared with increasing reaction time. No band at ~3680 cm^{-1} was detected in the reaction products that would indicate the presence of a trioctahedral smectite.

Atomic Force Microscopy (AFM)

An AFM image of Na-saturated smectite particles after 150 days reaction time is shown in Figure 7. The AFM analysis of the initial and the reacted particles indicate no major morphological changes throughout the experiment. Therefore, the following description includes all samples. The particles consist of irregular- and fine-grained plates. Mostly the edges are rounded, but straight edges appear as well. The top view shape of most particles resembles an ellipse, as already observed by Metz et al. (2005b) for the SAz-1 smectite. The height and the surface area of each of the selected particles were measured. A total of 400 heights and 350 surface area measurements were performed. The distribution of the height measurements for the initial smectite and the Reactor 6: 150 days sample show no change in particle morphology, particle height, and surface area. The number of layers in the smectite particles was calculated assuming that the thickness of a single TOT layer with the hydrated Na^+ layer was about 12.5 Å (Jasmund and Lagaly 1993). Because diluted smectite suspensions were used and the samples were dispersed during the preparation for the AFM measurements, the majority of the particles consists of 1–5 TOT layers (Fig. 7).

Oxygen-isotope analyses

The oxygen-isotope composition of the Na^+-saturated clays was monitored to provide another measure of reaction progress and is shown for the initial and the reacted smectites in Figure 8. The $\delta^{18}O$ values of the clays changed rapidly from 17.4‰ for the initial SAz-1 to 15.2‰ for the reacted smectite after 150 days. A similar trend was observed by Whitney and Northrop (1988) at higher temperatures (250–450 °C) for the SWy-1 smectite in distilled water. The composition of the water in the experiment was –7.5‰. The isotope values changed with time, decreasing rapidly in the beginning before attaining a value near 15.2‰, which shows only partial exchange with the aqueous solution oxygen. The initial exchange is most likely one of surface interaction. If significant dissolution-recrystallization was involved, one would expect greater exchange between solution and silicate material.

DISCUSSION

The major objective of the present study was to demonstrate changes in mineral structure of a smectite at low temperatures under conditions of high alkalinity. Other studies have been performed on similar material, but not at low temperature. Several different methods were used to obtain information on mineral evolution during the experiments.

Direct observation of crystal morphology

AFM observations of crystallite size, shape, and thickness supports the hypothesis that the process is dominated by solid-state transformation (Baronnet 1997). The materials appear to retain their outer morphology but change their internal crystallographic composition.

Measurements of structural change

XRD. In contrast to Whitney and Northrop (1988) and Bauer and Velde (1999), the initial and reacted smectites were measured in the Sr-saturated state at a fixed relative humidity. Under these conditions, misinterpretation of dehydrated layers for illite layers can be neglected. XRD and infrared spectra gave little evidence for a change in smectite mineralogy in our experiments. The number of expandable layers with one water layer increases, whereas the portion of the dehydrated layers is about constant with reaction time. This suggests an increase in overall layer charge on the smectite. The peak width of the (001) reflections increases with reaction time suggesting a decrease in the average diffracting domain. The peak position of the (060) band increases,

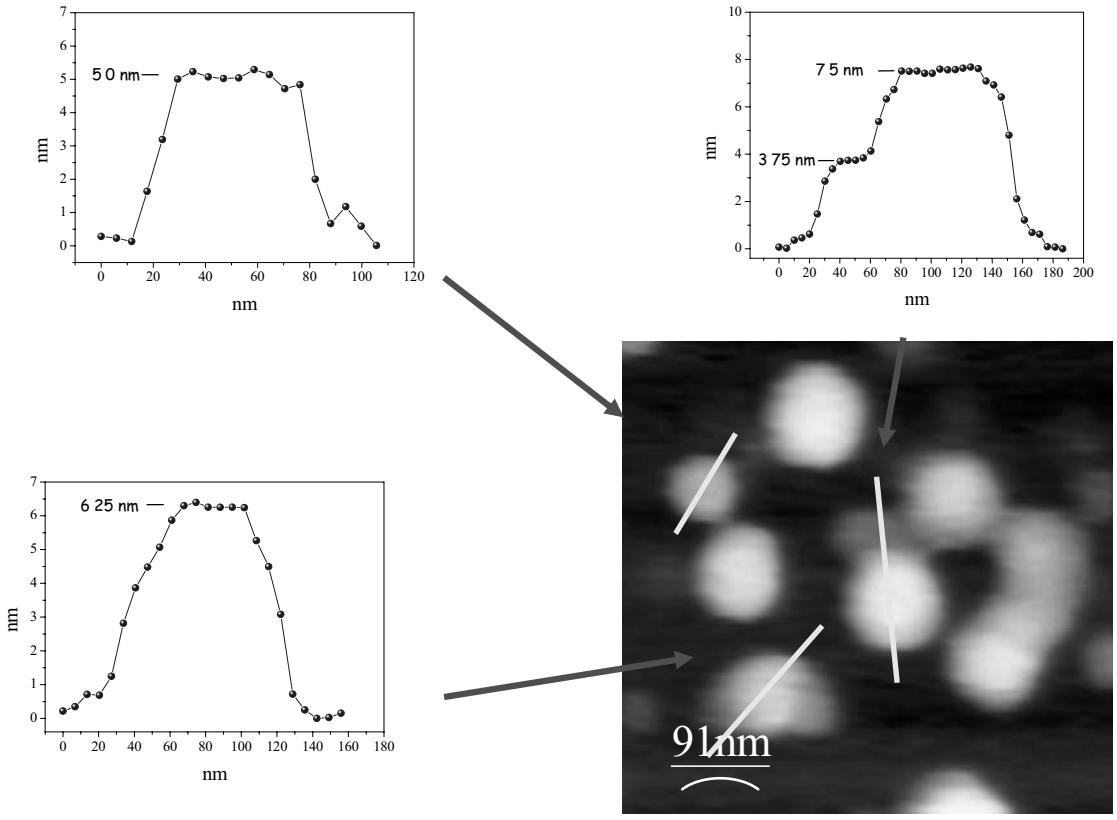

FIGURE 7. An AFM image of Na-saturated smectite particles in Reactor 6: 150 days. The particles consist of irregular and fine-grained plates with rounded edges. The three graphs show that the particles consist of 1–5 TOT layers.

suggesting a change in internal mineral composition and an increase in charge on the structures. The layer charge using XRD and alkyl-ammonium treatments was found to increase from 0.32 to 0.42, and a clear shift in the layer charge distribution toward high-charge layers was observed. Small amounts of trioctahedral mineral clusters were apparent [from (060) peak measurements], which indicates an increase of Mg in the smectite.

MS measurements. The dehydroxylation temperature decreased from 643 to 605 °C. This shift confirms the increased layer charge of the smectite. A lower dehydroxylation temperature for smectites with higher layer charge was observed by Schultz (1969) and Michot et al. (2005). In smectites, the octahedral sheet tends to be cis-vacant whereas the illites have mainly trans-vacant dispositions (Drits et al. 1998). It is evident that the reacted smectite has a different disposition of the hydroxyl groups, but that the *cis*-vacant character of the octahedral sheet remained nearly unchanged throughout the experiment. A second but small dehydroxylation appeared at 790 °C. A similar observation was made by Emmerich et al. (2001) for a de- and rehydroxylated Na-saturated cv smectite. XRD measurements of the (060) reflection indicate the appearance of trioctahedral Mg-smectite layers, which is consistent with the XPS data showing an increase of Mg in the smectite structure (Fig. 5) and XRD data for the (060) peak indicating a small amount of a trioctahedral phase.

MS curves for the Na-saturated samples SAz-1 and the resaturated Reactor 6: 150 days sample are shown in Figure 6. The amount of adsorbed water depends on the nature of the interlayer cations, the pre-treatment of the sample, and the silica lattice (Grim 1968). Two types of water molecules can be distinguished in the interlayer space of smectites: filling water that belongs to outer hydration shells of the cations or is bound to the surface of the smectite layers; and water belonging to the first hydration shell of the exchangeable cations.

Both smectites in Figure 6 have the same interlayer cation and the same pre-treatment so that the differences can be attributed to changes in the silica lattice and, as a consequence, in the number of interlayer cations. It is evident that with increasing layer charge, more cations are needed to compensate the charge deficit. This was confirmed by TG measurements that indicate an increase of the interlayer water from 12 to 17% after 150 days of reaction time corresponding to increase of about 8 to 10 water molecules per cation Na^+. These numbers are within the range of the values for Na^+-saturated saponites dominated by 2W layers (Michot et al. 2005). This is an important observation because it means that the hydration sphere of the Na^+ cations is already sufficient to induce the major presence of 2W layers from the beginning. This means that additional H_2O molecules are not strongly bound to interlayer cations; in turn, they should be easier to remove. The relative proportion of 1W layers increases at the expense of 2W layers concurrently with the increase of water content. This apparent contradiction is likely related to a more complete filling of the first water layer (Meunier 2005) in the reacted samples. The more "stable" character of 1W layers

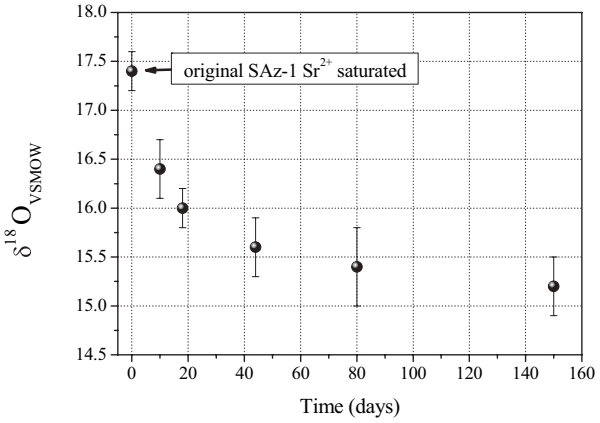

FIGURE 8. Plot of the evolution of the $\delta^{18}O$ VSMOW values as a function of reaction time. Error bars correspond to the standard deviation of triplicates.

in reacted samples is possibly linked to the increased amount of tetrahedral charges and thus to the strong undersaturation of surface O atoms that in turn requires strong interactions with interlayer cations. In our experiments, the occurrence of a second dehydration reaction centered at 127 °C after 150 days was observed, in addition to the 150 °C maximum (Fig. 6). This behavior is consistent with the water vapor adsorption-desorption isotherms reported by Michot et al. (2005) that showed a transition toward higher hydration states at lower P/P_0 values. As we know, hydrated smectites consist of %2W, %1W, and %0W layers that superimpose in one peak that is often not resolved in DSC or MS curves. Water adsorbed on clay surfaces, especially in generated pores or at least on enlarged outer surfaces as proposed by Michot et al. (2005), explains the STA dehydration results, which indicate an increased amount of more loosely bound water that does not contribute to the observed swelling but to the overall water content.

Measurements of chemical change

Oxygen constitutes the structural skeleton of the reacting materials, and the degree of isotopic resetting can be used to indicate the extent of rearrangement of the mineral structure at high temperatures (Whitney and Northrop 1988). The initial rapid shift in $\delta^{18}O$ values from 2.2‰ to more negative values for the reacted smectites is in agreement with an exchange of structural surface oxygen with water/KOH oxygen. This is due to the negative $\delta^{18}O$ value of the exchange fluid (–7.4‰). According to Kohn and Valley (1998) and Sheppard and Gilg (1996) for temperatures of 80 °C, a fractionation of around +19‰ for smectite–fluid exchange applies, which would yield an end value of +12‰ for a smectite in equilibrium with the fluid. Because at a solid/liquid ratio of 1/80, the $\delta^{18}O$ value of the liquid can be regarded as constant throughout experimental run time, the rapid initial shift of the oxygen isotope ratio is followed by a decrease in reaction rate with time in the reacted smectites. The isotope data can be taken to indicate a rapid equilibration of the solids with the aqueous solution, which would indicate no significant recrystallization of the smectite material.

XPS data showed that the increase of Al in the structure (increase of the Al/Si ratio from 0.39 to 0.48) is responsible for the increase in the layer charge. This is consistent with the solution chemistry that indicates an increase in Si in solution relative to Al.

Chemical measurements of dissolved species and oxygen isotopes of solids indicates that little dissolution occurred but significant change in the overall composition of the solids is seen through changes in solution composition.

Comparison with previous experiments

Our results are consistent with previous studies that were conducted at neutral pH and higher temperatures (100 and 250 °C) with various sources of K. Howard and Roy (1985) found the formation of high-charged layers when montmorillonite reacted at 150 and 250 °C. Eberl et al. (1978) and Whitney (1992) found that the formation of high-charge layers is promoted by an increase of K in the system. Yamada and Nakasawa (1993) observed the formation of a beidellite + saponite assemblage after the experimental alteration of synthetic beidellite-montmorillonite mixed-layers at high temperatures. During montmorillonite alteration at 100 and 200 °C, Beaufort et al. (2001) observed the formation of trioctahedral Mg-smectite and high-charge beidellitic layers. The beidellite + saponite assemblage is also observed between 100–200 °C in active geothermal fields where montmorillonite seems to be no longer stable at temperatures >100 °C (Beaufort et al. 1995).

Process of mineral change

The observations cited above indicate that there is a significant, gradual change in the mineral cation composition of the 2:1 layers of smectite in the presence of a KOH solution. The smectite minerals become highly charged and have smaller coherent diffracting domains. These changes involve significant chemical modifications within the crystallites. Aluminum substitutes for Si and Mg for Al to a significant degree. The question is then: How does this happen? Essentially two pathways can be proposed according to classical theories: dissolution/crystallization or solid-state transformation.

If dissolution/precipitation is not the mechanism of mineral chemical change, one must accept a mechanism of diffusive modification within the existing crystallites. This change occurs at low temperatures, 80 °C. Such a conclusion is surprising, given the assumed very low rate of ionic diffusion in silicate crystallites at low temperatures (Kyser and Kerrich 1991). However, the experimental evidence shown here strongly rejects the hypothesis of significant dissolution and crystallization, the other alternative to mineral change in aqueous solutions.

The conclusion that a diffusion mechanism induces mineral change at low temperatures is surprising. Yet, if one considers the great complexity and range of solid solution common in low temperature clay minerals, one can suspect that important mineral compositional changes occur at these low temperatures. Normally, one attributes high solid solutions in solids to high thermal energy but it is known that chemical variability can also increase at lower temperatures in systems such those where illite is stable (Velde 1985).

We propose that the phenomenon of chemical change at low temperatures is one of a response to new chemical

conditions inducing a larger range in chemical composition that, in the case studied, increases the Al and Mg content of the observed smectite minerals. In this particular instance, the change is accomplished by internal diffusion within the smectite crystallites. This process can be seen as a rupture of homogeneity within the smectite crystals that creates smaller coherent diffraction domains without necessitating a complete dissolution–re-crystallization of the silicate framework.

ACKNOWLEDGMENTS

We thank Klaus Spieler and Eva Soballa (INE) for their technical assistance during the SEM measurements We thank Heike Pieper and Dirk Bosbach for their help performing the AFM measurements The present manuscript was improved by the constructive reviews of Victor A Drits, Hanan J Kisch, Alain Meunier, and the Associate Editor Kevin Rosso

REFERENCES CITED

Altaner, S P and Ylagan, R F (1997) Comparison of structural models of mixed-layer illite/smectite and reaction mechanisms of smectite illitization Clays and Clay Minerals, 45, 517–533

Awwiller, D N (1993) Illite/smectite formation and potassium mass transfer during burial diagenesis of mudrocks: a study from the Texas Gulf Coast Paleocene-Eocene Journal of Sedimentary Petrology, 63, 501–512

Baronnet, A (1997) Silicate microstructures at the sub-atomic scale Comptes Rendus de l'Academie des Sciences, Serie IIa, 324, 157–172

Bauer, A and Velde, B (1999) Smectite transformation in high molar KOH solutions Clay Minerals, 34, 259–273

Beaufort, D , Papapanagiotou, P , Patrier, P , and Traineau, H (1995) Les interstratifies I-S et C-S dans les champs géothermiques actifs: sont-ils comparables ceux aux séries diagénétiques? Bulletin des Centres de Recherches Exploration-production Elf Aquitaine Elf Aquitaine Prod , 19, 267–294

Beaufort, D , Berger, G , Lacharpagne, J C , and Meunier, A (2001) An experimental alteration of montmorillonite to a di + trioctahedral smectite assemblage at 100 and 200 degrees C Clay Minerals, 36, 211–225

Brindley, G W and Brown, G (1980) Crystal Structures of Clay Minerals and their X-ray Identification, p 125–195 Mineralogical Society, London

Clayton, R N and Mayeda, T K (1963) The use of bromine pentafluoride in the extraction of oxygen from oxides and silicates for isotopic analysis Geochimica Cosmochimca Acta, 27, 43–52

Cuadros, J and Altaner, S P (1998) Characterization of mixed-layer illite-smectite from bentonites using microscopic, chemical, and X-ray methods: Constraints on the smectite-to-illite transformation mechanism American Mineralogist, 83, 762–774

Day, P R (1965) Particle Fractionation and particle size analysis In C A Black, Ed , Methods of Soil Analysis, p 545–567 American Society of Agronomy, Madison, Wisconsin

Drits, V A (1985) Mixed-layer minerals: Diffraction methods and structural features In L G Schultz, H Van Olphen, and F A Mumpton, Eds , International Clay Conference, p 33–45 Clay Minerals Society, Denver, Colorado

Drits, V A and Sakharov, B A (1976) X-ray structure analysis of mixed-layer minerals 256 p Doklady Akademii Nauk SSSR, Moscow

Drits, V A , Besson, G , and Muller, F (1995) An improved model for structural transformations of heat-treated aluminous dioctahedral 2:1 layer silicates Clays and Clay Minerals, 43, 718–731

Drits, V A , Lindgreen, H , Sakharov, B A , and Salyn, A S (1997) Sequence structure transformation of illite-smectite-vermiculite during diagenesis of Upper Jurassic shales, North Sea Clay Minerals, 33, 351–371

Drits, V A , Eberl, D D , and Srodon, J (1998) XRD measurement of mean thickness, thickness distribution and strain for illite and illite-smectite crystallites by the Bertaut-Warren-Averbach technique Clays and Clay Minerals, 46, 38–50

Dunoyer de Segonzac, G (1970) The transformation of clay minerals during diagenesis and low-grade metamorphism: A review Sedimentology, 15, 281–346

Eberl, D D , Whitney, G , and Khoury, H (1978) Hydrothermal reactivity of smectite American Mineralogist, 63, 401–409

Eberl, D D , Srodon, J , and Northrop, H R (1986) Potassium Fixation in Smectite by Wetting and Drying Acs Symposium Series, 323, 296–326

Eberl, D D , Velde, B , and Mc Cormick, T (1993) Synthesis of illite-smectite from smectite at Earth surface temperatures and high pH Clay Minerals, 28, 49–60

Emmerich, K , Plotze, M , and Kahr, G (2001) Reversible collapse and Mg^2 release of de- and rehydroxylated homoionic *cis*-vacant montmorillonites Applied Clay Science, 19, 143–154

Ferrage, E (2004) Etude expérimentale de l'hydratation des smectites par simulation des raies 00l de diffraction des rayons X Implications pour l'étude d'une perturbation thermique sur la minéralogie de l'argilite du site Meuse-Haute Marne , p 321 Université Joseph Fourier, Grenoble

Ferrage, E , Lanson, B , Sakharov, B A , and Drits, V A (2005) Investigation of smectite hydration properties by modeling experimental X-ray diffraction patterns: Part I Montmorillonite hydration properties American Mineralogist, 90, 1358–1374

Grim, R E (1968) Clay Mineralogy McGraw-Hill Book Company, New York

Hofmann, H , Bauer, A , and Warr, L N (2004) Behaviour of smectite in strong salt brines under conditions relevant to the disposal of low- to medium-grade nuclear waste Clays and Clay Minerals, 52(1), 14–24

Howard, J J and Roy, D M (1985) Development of layer charge and kinetics of experimental smectite alteration Clays and Clay Minerals, 33, 81–88

Hower, J , Eslinger, E V , Hower, M E , and Perry, E A (1976) Mechanism of burial metamorphism of argillaceous sediment: 1 Mineralogical and chemical evidence Geological Society of America Bulletin, 87, 725–737

Jasmund, K and Lagaly, G (1993) Tonminerale und Tone Struktur, Eigenschaften, Anwendung und Einsatz in Industrie und Umwelt 490 p Steinkopff Verlag, Darmstadt

Jaynes, W F and Bigham, J M (1987) Charge reduction, octahedral charge, and lithium retention in heated, Li-satured smectites Clays and Clays Minerals, 35, 440–448

Johnson, J W , Oelkers, E H , and Helgeson, H C (1992) Supcrt92—a Software Package for Calculating the Standard Molal Thermodynamic Properties of Minerals, Gases, Aqueous Species, and Reactions from 1 to 5000 bars and 0 to 1000 °C Computers and Geosciences, 18, 899–947

Kohn, M J and Valley, J W (1998) Oxygen isotope geochemistry of the amphiboles: Isotope effects of cation substitutions in minerals Geochimica et Cosmochimica Acta, 62, 1947–1958

Kyser, T K and Kerrich, R (1991) Retrograde exchange of hydrogen isotopes between hydrous minerals and water at low temperatures In H P J Taylor, J R O'Neil, and I R Kaplan, Eds , Stable Isotope Geochemistry: A tribute to Samuel Epstein, Special Publication 3, p 409–422 Geochemical Society, Washington, D C

Madejova, J and Komadel, P (2001) Baseline studies of The Clay Minerals Society Source Clays: Infrared methods Clays and Clay Minerals, 49, 410–432

Mermut, A R and Lagaly, G (2001) Baseline studies of The Clay Minerals Society Source Clays: Layer-charge determination and characteristics of those minerals containing 2 : 1 layers Clays and Clay Minerals, 49, 393–397

Metz, V , Amram, A , and Ganor, J (2005a) Stoichiometry of smectite dissolution Geochimica Cosmochimica Acta, 69, 1755–1772

Metz, V , Raanan, H , Pieper, H , Bosbach, D and Jiwchar, G (2005b) Towards the establishment of a reliable proxy for the reactive surface area of smectite Geochimica et Cosmochimica Acta, 69, 2581–259

Meunier, A (2005) Clays, 472 p Springer, Berlin

Meunier, A , Lanson, B , and Beaufort, D (2000) Vermiculitization of smectite interfaces and illite layer growth as a possible dual model for illite-smectite illitization in diagenetic environments: a synthesis Clay Minerals, 35, 573–586

Michot, L J , Bihannic, I , Pelletier, M , Rinnert, E , and Robert, J L (2005) Hydration and swelling of synthetic Na-saponites: Influence of layer charge American Mineralogist, 90, 166–172

Moore, D M and Reynolds, R C (1997) X-ray Diffraction and the Identification and Analysis of Clay Minerals Oxford University Press, New York

Nadeau, P H and Bain, D C (1986) Composition of Some Smectites and Diagenetic Illitic Clays and Implications for Their Origin Clays and Clay Minerals, 34, 455–464

Robertson, H E and Lahann, R W (1981) Smectite to illite conversion rates: Effects of solution chemistry Clays and Clay Minerals, 29, 129–135

Sakharov, B A and Drits, V A (1973) Mixed-layer kaolinite-montmorillonite: A comparison of observed and calculated diffraction patterns Clays and Clay Minerals, 21, 15–17

Sakharov, B A , Lindgreen, H , and Drits, V A (1999a) Mixed-layer kaolinite-illite-vermiculite in North Sea shales Clay Minerals, 34, 333–344

Sakharov, B A , Lindgreen, H , Salyn, A , and Drits, V (1999b) Determination of illite-smectite structures using multispecimen XRD profile fitting Clays and Clays Minerals, 47, 555–566

Savin, S M , and Epstein, S (1970) The oxygen and hydrogen isotope geochemistry of clay minerals Geochimica Cosmochimica Acta, 34, 25–42

Schultz, L G (1969) Lithium and potassium absorption, dehydroxylation temperature, and structural water content of aluminous smectites Clays and Clays minerals, 17, 115–149

Sheppard, S M F and Gilg, H A (1996) Stable isotope geochemistry of clay minerals Clay Minerals, 31, 1–24

Shutov, V D , Drits, V A , and Sakharov, B A (1969) On the mechanism of a postsedimentary transformation of montmorillonite into hydromica In L Heller, Ed , International Clay Conference, p 523–531 Israel University Press, Jerusalem

Srodon, J , Morgan, D J , Eslinger, E V , Eberl, D D , and Karlinger, M R (1986) Chemistry of illite/smectite and end-member illite Clays and Clay Minerals,

34, 368–378
Velde, B (1985) Clays Minerals: A physico-chemical explanation of their occurrence, 427 p Elsevier, Amsterdam
Whitney, G (1992) Dioctahedral smectite reactions at elevated temperatures: Effects of K-availability, Na/K ratio, and ionic strength Applied Clay Science, 7, 97–112
Whitney, G and Northrop, H R (1988) Experimental investigation of the smectite to illite reaction: Dual reaction mechanisms and oxygen-isotope systematics American Mineralogist, 73, 77–90
Wolery, T J , Jackson, K J , Bourcier, W L , Bruton, C J , Viani, B E , and Delany, J M (1988) The Eq3/6 Software Package for Geochemical Modeling—Current Status Abstracts of Papers of the American Chemical Society, 196, 23-GEOC
Yamada, H and Nakasawa, H (1993) Isothermal treatments of regularly interstratified montmorillomite-beidellite at hydrothermal conditions Clays and Clay Minerals, 41, 726–730